Journal of Solid State Electrochemistry
https://doi.org/10.1007/s10008-018-3995-y

ORIGINAL PAPER

Photoelectrochemical performance of dye and semiconductor sensitization on 1-D hollow hexagonal ZnO rods: A comparative study

S. S. Patil[1] · N. L. Tarwal[1] · H. M. Yadav[2] · S. D. Korade[1] · T. S. Bhat[1] · A. M. Teli[1] · M. M. Karanjkar[3] · J. H. Kim[4] · P. S. Patil[1]

Received: 1 February 2018 / Revised: 12 May 2018 / Accepted: 14 May 2018

Abstract

One-dimensional hollow hexagonal ZnO rods (1-D HHZRs) were grown onto the SnO_2: F (FTO) coated glass substrates by using two-step deposition techniques. Initially, the ZnO seed layer was coated onto the FTO which was followed by hydrothermal route in order to grow 1-D HHZRs. These 1-D HHZRs were decorated with Eosin-Y dye and CdS semiconductor nanoparticles (NPs) by using a chemical routes like dip coating and successive ionic layer absorption reaction (SILAR) technique, respectively to improve its photoelectrochemical (PEC) performance. The structural, morphological, optical and electrochemical characterizations of the thin films were analyzed by various sophisticated instruments. X-ray diffraction (XRD) pattern corroborated the phase formation of ZnO and CdS with the hexagonal and cubic crystal structure, respectively. 1-D HHZRs films were obtained by scanning electron microscopy (SEM) with rod diameter of about 1.47 μm. Furthermore, SEM image clearly showed the CdS NPs covered 1-D HHZRs. The direct optical bandgap energy of the samples were estimated to be 3.28, 3.24 and 3.03 eV. CdS NPs-sensitized 1-D HHZRs samples showed hydrophilic nature for water contact angle, which is advantageous for the better improvement in the PEC performance as compared with pristine and dye-sensitized 1-D HHZRs.

Keywords ZnO · 1-D hollow hexagonal rods · CdS · Mott-Schottky · Solar cell

Introduction

In recent years, tremendous energy is required due to the industrial revolution, so renewable energy sources need to be studied. In particular, solar energy is easily available, and it is easy to convert into electricity as compared with other renewable sources [1]. Here, the efficiency of solar cell is an important factor which should be taken into consideration. The researchers are engaged in developing thin films for more efficient solar cell application [2].

Among several oxides, zinc oxide (ZnO) thin films attract more interest due to their versatile properties such as high electron mobility, good transparency and a wide direct bandgap ~3.37 eV [3]. Therefore, ZnO structures have been used for various applications such as fabrication of various sensors, self-cleaning glasses [4], light-emitting devices, optoelectronics [5], solar cells [6] and biomedical applications. ZnO thin films with diverse morphologies have been produced by a wide range of growth techniques, such as chemical bath deposition (CBD) [7], sol-gel [8], spin coating [9], chemical vapor depositions (CVD) [10], spray pyrolysis [11], etc. Among them, wet chemical method is an easy and cost-effective commercial technique to prepare ZnO thin films with desirable properties.

The semiconductor-sensitized solar cells (SSSCs) belong to the third generation of solar cells, which represent solar cells with low manufacture cost and satisfactory efficiency.

✉ J. H. Kim
jinhyeok@chonnam.ac.kr

✉ P. S. Patil
patilps_2000@yahoo.com

[1] Thin Film Materials Laboratory, Department of Physics, Shivaji University, Kolhapur, Maharashtra 416 004, India

[2] Department of Energy and Materials Engineering, Dongguk University, Seoul 04620, South Korea

[3] Department of Physics, Vivekanand College, Kolhapur, Maharashtra 416 003, India

[4] Department of Materials Science and Engineering, Chonnam National University, Gwangju 500 757, South Korea

Published online: 08 June 2018

SSSCs have recently attracted significant attention as a promising alternative to the dye-sensitized solar cells (DSSCs) due to their distinctive characteristics such as higher intrinsic dipole moment favoring charge separation, large extinction coefficient and multiple exciton generation etc. [12]. Moreover, the operational principle of the SSSC is very analogous to DSSC, only the light-absorbing dye is exchanged by inorganic semiconductor nanomaterials [13, 14].

Among the best performing semiconductor sensitizers, CdS is a catchy choice. It is extensively used due to its direct small bandgap of 2.4 eV [15], capability to grow with numerous easy chemical methods, and higher conduction band edge (~ 4.3 eV) related to ZnO (~ 4.1 eV in a vacuum). The ZnO/CdS heterostructure forms a type-II band configuration which helps to shrink the rate of recombination among electron-hole pairs due to injection of high-energy electrons from CdS to ZnO [16].

One-dimensional (1-D) structures are more advantageous for solar cell application as they provide an ideal direct pathway for charge transport with a large surface area. If the electrons are trapped in the surface states of the absorbing semiconductor (CdS), their lifetime in that absorbing semiconductor increases, which boosts the probability of recombination with the electrolyte species. The 1-D structures of wide band gap semiconductors (WBSCs) helps by virtue of low scattering and recombination probability. Owing to direct pathways; photogenerated charge carriers to be transported through the ordered rods or tubes [17]. The electron transportation in the crystalline ZnO rods is expected to be several orders of magnitude quicker than a random polycrystalline network of other WBSCs [18].

Several results have been reported on ZnO based DSSCs and SSSCs separately, but to the best of our knowledge, very few reports are available on the comparative study of pristine ZnO, dye and semiconductor sensitized ZnO. Therefore, the challenge is to find out the best photoelectrochemical (PEC) performance among the dye and semiconductor sensitized hollow hexagonal ZnO rod (HHZRs) samples. In the present investigation, we report an easy, two-step chemical approach for synthesizing the hollow hexagonal ZnO rods. Further, these samples are used for Eosin-Y dye and CdS semiconductor nanoparticles (NPs) sensitization. The main objective of this study is to see the effect of Eosin-Y dye and CdS NPs sensitization to HHZRs. Moreover, the PEC performance of all the samples are investigated and reported here.

Experimental procedure

All chemical reagents and fluorine-doped tin oxide (FTO ~ 15 Ω cm^{-2}) substrates used in this synthesis were bought from Sigma Aldrich. All the chemicals were used without further purification.

Synthesis of 1-D HHZRs thin films

Initially, the seed layer of ZnO was prepared by dipping FTO substrates in 0.025 M zinc acetate solution in ethanol for 20 s and the films were allowed to keep on drying for 12 h. Then, these films were annealed at 300 °C for 10 min. Furthermore, for growing the 1-D HHZRs, these seed coated films were kept at 90 °C for 6 h in hydrothermal autoclave with 200 ml solution of zinc acetate ($Zn(CH_3CO_2)\cdot 2H_2O$) in a mixture of double distilled water (DDW) and hexamine (HMTA) (1:1, volume ratio) with equimolar concentration of 0.05 M. The prepared samples of ZnO were denoted as Z_1 and used for further synthesis.

Synthesis of dye-sensitized HHZRs thin films

The dip coating method was used for the effective dye loading over Z_1 sample. The Z_1 sample was dipped in 0.3 mM Eosin-Y dye solution in ethanol for 24 h at room temperature. Finally, the films were rinsed carefully with ethanol and kept for drying at room temperature.

Synthesis of semiconductor sensitized HHZRs thin films

A simple SILAR method was used to sensitize CdS NPs on ZnO thin films. The Z_1 sample was placed into an aqueous solution of 0.01 M $CdCl_2$, washed with DDW, again immersed in aqueous 0.01 M Na_2S solution and again washed with DDW. The Z_1 film was immersed in cationic and anionic bath for 10 s and in DDW for 20 s to complete one SILAR cycle. Upon the completion of 20 cycles, the deposited films were rinsed with ethanol and air dried at room temperature.

The pristine 1-D HHZRs, Eosin-Y dye, and CdS NPs sensitized 1-D HHZRs thin film samples were denoted as Z_1, Z_2 and Z_3, respectively and these samples were used for further characterizations.

Characterizations

The structural properties of films were studied by X-ray powder diffractometer with Cu K_α = 1.54056 Å (Bruker AXS Analytical Instruments Private Ltd., Germany, Model: D2 phaser). The surface morphology and cross-sectional images were obtained by scanning electron microscopy (SEM) (JEOL JSM-6360). The optical absorption spectra were recorded over the wavelength range of 350–750 nm by a UV–Vis-NIR spectrophotometer (UV1800, Shimadzu, Japan). The contact angle study was analyzed through Holmarc's contact angle meter model no.: HO-IAD-CAM-01B equipment with CCD camera. The PEC investigations of films were performed via AUTOLAB PGSTAT100 FRA 32 potentiostat in the two-electrode system, under the illumination of a tungsten

lamp (20 mW cm^{-2}). The active area of the thin film used for PEC measurement was 1 cm^2.

Results and discussion

X-ray diffraction

Figure 1 shows XRD patterns of Z_1 and Z_3 samples while the vertical lines show the standard JCPDS peaks. In the XRD pattern, Z_1 thin film shows hexagonal structure having a highest intense peak observed at 34.49° which corresponds to (002) plane. Besides this major peak, ten more peaks corresponding to (100), (101), (102), (110), (103), (200), (112), (201), (004) and (202) planes are observed at 31.81°, 36.17°, 47.58°, 59.69°, 62.9°, 66.41°, 67.92°, 69.11°, 72.55° and 76.96°, respectively. The obtained XRD patterns are exactly matched with the standard JCPDS card number 01-079-0206. The sharp and intense peak at 34.49° with (002) orientation of ZnO confirms the formation of 1-D rods [19].

In case of the Z_3 sample, XRD pattern shows peaks of both ZnO and CdS. The peaks appeared at 26.61° and 54.64° correspond to the (111) and (222) planes shows the presence of CdS which shows the cubic crystal structure. The XRD peaks of CdS are well matches with JCPDS card number 01-080-0019. The peaks marked with Δ belong to CdS peaks and the peaks denoted by an asterisk belong to FTO substrate in the XRD patterns. There are no any other impurity peaks detected in the XRD patterns which indicates the purity of the samples. The crystallite sizes for both the samples are calculated by using Scherrer formula [20],

$$D = \frac{0.9\,\lambda}{\beta\cos\theta} \tag{1}$$

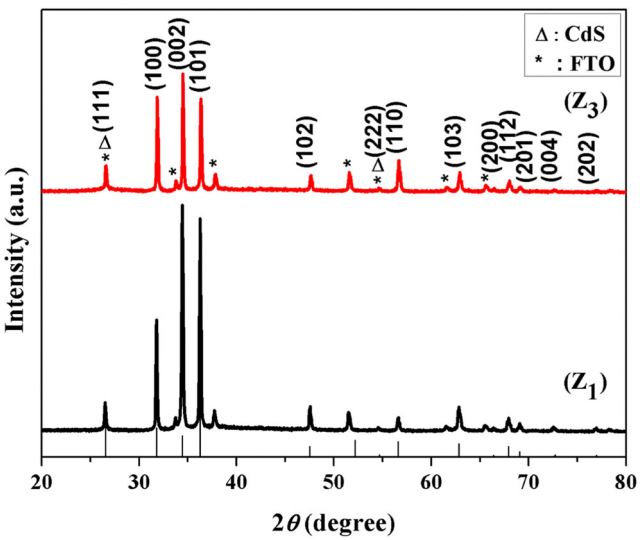

Fig. 1 X-ray diffraction patterns of Z_1 and Z_3 samples and the vertical lines show the standard JCPDS peaks

The calculated crystallite sizes for the Z_1 and Z_3 samples were found to be 81 and 101 nm, respectively.

Scanning electron microscopy

Figure 2 shows the obtained SEM images for Z_1, Z_2 and Z_3 samples and *Inset* shows corresponding cross-sectional images. It is seen that the uniformly distributed vertically aligned 1-D HHZRs are fully covered over the substrate. Figure 3 shows the graphical representation of CdS NPs decorated 1-D HHZRs. The average diameter of the hollow ZnO rods is ~ 1.47 μm for all Z_1, Z_2 and Z_3 samples. The Z_3 sample shows uniform distribution or anchoring of CdS NPs over and in between the interspacing of HHZRs with the size of ~ 50 nm.

UV–Vis-NIR spectroscopy

Figure 4 shows the optical absorption spectra of Z_1, Z_2 and Z_3 samples. The optical absorption spectra of all samples were recorded in the wavelength range of 350 to 750 nm. The absorption edge of Z_1 sample is observed at 378 nm, which indicates that the material is active in the UV region of the solar spectrum. The absorption peak of Z_2 sample is present at 524 nm. Also, the absorption edge for Z_3 sample is shifted towards higher wavelength and is present at 409 nm along with the CdS absorption edge at 605 nm. This is due to the sensitization of CdS semiconductor NPs over 1-D HHZRs. These sensitization helps to absorb the photons in the UV as well as the visible region of the electromagnetic solar spectrum.

The nature of optical transition and the exact value of the optical bandgap of the material can be acquired using optical absorption measurements. The optical bandgap energy has been evaluated by using the relation [21],

$$\frac{ah\nu}{t} = A\left(E_g - h\nu\right)^n \tag{2}$$

where a is the absorption coefficient, t is the thickness of the thin film, ν is the frequency of the incident radiation, A is constant, E_g is the bandgap energy of the material, h is the Planck's constant and n is a constant, which has values $\frac{1}{2}, \frac{3}{2}$, 2 and 3 be influenced by nature of electronic transition responsible due to the absorption of light radiations. $n = \frac{1}{2}$ for permitted direct transition, $n = \frac{3}{2}$ for prohibited direct transition, $n =$ 2 for permitted indirect transition, and $n = 3$ for prohibited indirect transition [22]. In this work, $n = \frac{1}{2}$ for the direct transition. *Inset* of Fig. 4 shows the plot of $(\alpha h\nu)^2$ versus photon energy of $h\nu$ for Z_1, Z_2 and Z_3 where $\left(\alpha = \frac{a}{t}\right)$. The optical energy gap values for the prepared samples were calculated from this plot. Bandgap energies of the Z_1, Z_2 and Z_3 samples are found to be 3.28, 3.24 and 3.03 eV, respectively. This indicates that, as compare to Z_1, the bandgap of Z_2 and Z_3 is reduced due to the sensitization of Eosine-Y dye and CdS NPs

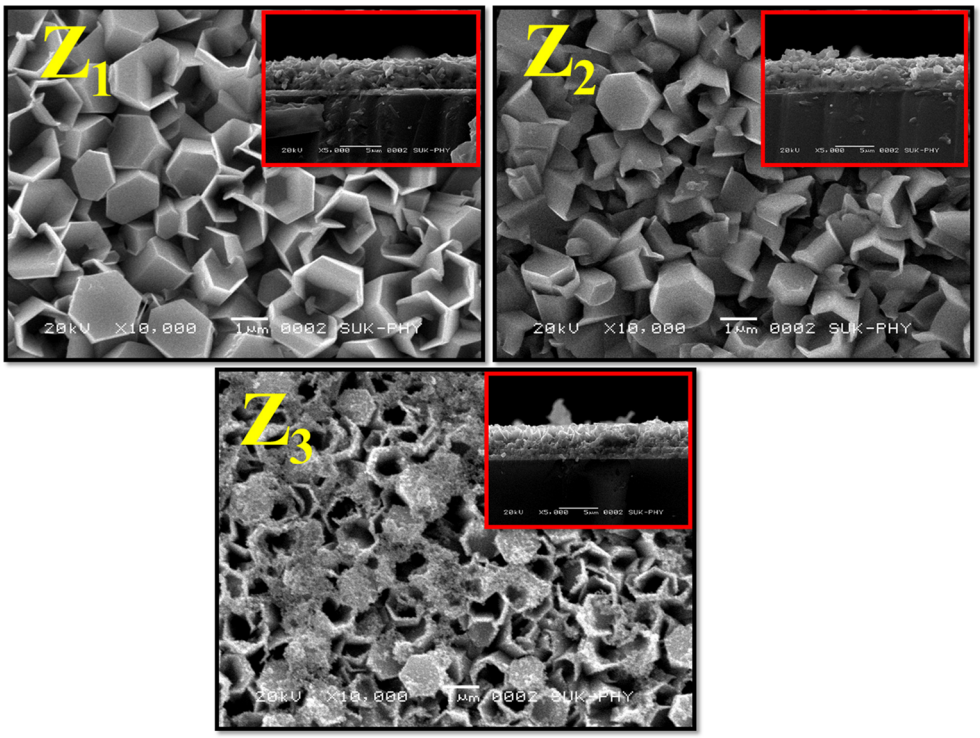

Fig. 2 Scanning electron microscopy images of Z_1, Z_2 and Z_3 thin films. *Inset* shows the cross-sectional images of the respective samples

respectively over 1-D HHZRs, and it is helpful for the better light absorption.

Surface wettability test

In the present case, surface wettability test was carried out to obtain the values of the water contact angle of the thin films. The obtained values of water contact angle are 70°, 35° and 18° for Z_1, Z_2 and Z_3 thin film samples, respectively in Fig. 5. Here, CdS sensitized 1-D HHZRs sample has low contact angle as compared with all the samples. This may be due to the strong cohesive force among the water droplet and Z_3 film. Hence, it shows a hydrophilic nature. This can assist the contact among electrolyte and film surface which permits at ease diffusion of ions between them. Due to which, the liquid is attracted rather than repelled by the film. This specific property is beneficial for making intimate contact of an aqueous electrolyte with electrode surface in the photo-electrochemical cell. We believe that this specific property will tentatively reveal the viability of Z_3 film in electrolyte/electrode boundary for improved performances [23].

PEC measurements

For *I–V* measurements, the following two electrode cell configurations were used to record *I–V* plots and the cell configurations are as shown below,

$$\text{Glass/FTO/1-DHHZRs/0.5 M } Na_2SO_4\text{/graphite} \quad (3)$$

$$\text{Glass/FTO/Eosin-Y dye-sensitized 1-D HHZRs/0.1 M polyiodide/graphite} \quad (4)$$

$$\text{Glass/FTO/CdS NPs sensitized 1-D HHZRs/0.5 M polysulfide/graphite} \quad (5)$$

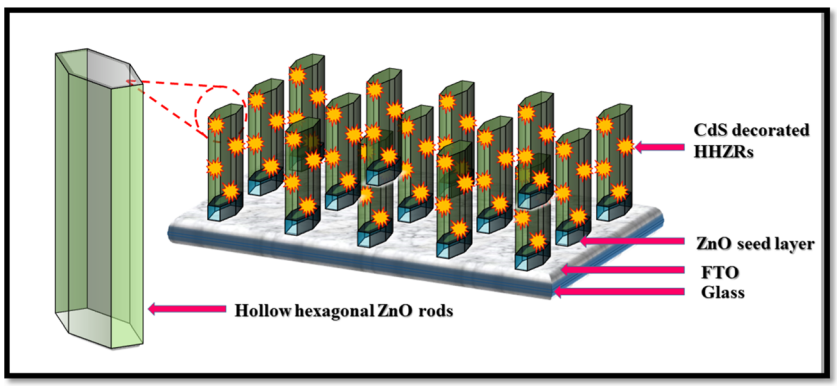

Fig. 3 Schematic diagram of CdS NPs decorated 1-D HHZRs

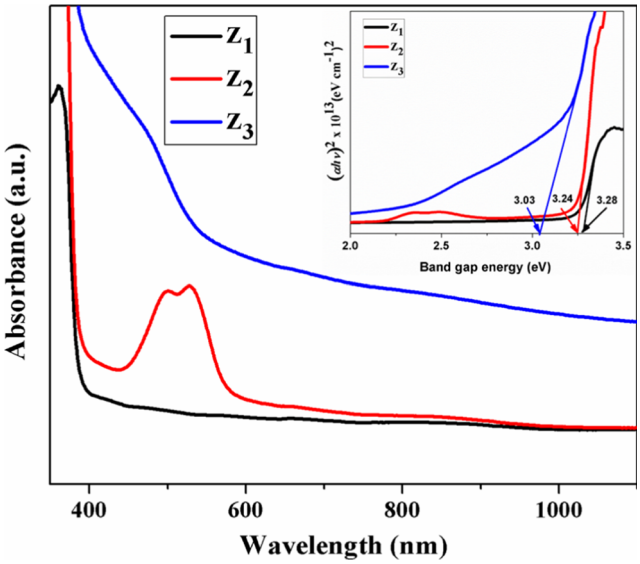

Fig. 4 The bandgap energy of ZnO samples (Z_1, Z_2 and Z_3). *Inset* shows the variation of absorbance versus wavelength of Z_1, Z_2 and Z_3 samples

For Z_1 configuration aqueous 0.5 M Na_2SO_4, Z_2 configuration 0.1 M polyiodide electrolyte is used. For this, potassium iodide, lithium iodide, and iodine granules (all 0.1 M concentration) in a solution of acetonitrile and propan-2-ol as 1:1 proportion is used, and the solution is stirred for 10 min. For the Z_3 configuration, 1 M polysulphide electrolyte is used. For this, 0.5 M sodium hydroxide, 0.5 M sodium sulfide flakes and 0.5 M sulfur metal powder were added into DDW and solution heated for 10 min. at 70 °C.

Figure 6 shows the final SSSC device comprising CdS NP sensitized 1-D HHZRs as a photoanode and graphite as a cathode. In between the photoelectrode and counter electrode, the polysulfide electrolyte was used. The schematic for Glass/FTO/CdS NPs sensitized 1-D HHZRs/polysulfide/graphite assembly is shown in Fig. 6. The PEC investigations were carried out and the measured. *I–V* characteristics of Z_1, Z_2 and Z_3 thin films are shown in Fig. 7. The magnitude of the I_{SC} are found to be 167, 318 and 558 μA cm^{-2} for the Z_1, Z_2 and Z_3 films, respectively. For the Z_3 sample, CdS absorption band edge shifted from UV to visible so more numbers of photons are absorbed that cause an increase in I_{SC}. The corresponding V_{OC} values are found to be 105, 190 and 423 mV for the Z_1, Z_2 and Z_3 films, respectively. The solar cell output parameters like fill factor (FF), efficiency (η), series resistance (R_S), and shunt resistance (R_{Sh}) for all the samples are calculated from Equations. (6) to (9), respectively [21].

$$FF = \frac{I_{max} \text{ x } V_{max}}{I_{sc} \text{ x } V_{oc}} \tag{6}$$

$$\eta = \frac{I_{sc} \text{ x } V_{oc}}{P_{in}} \; x \; FF \tag{7}$$

$$\left(\frac{dI}{dV}\right)_{I=0} = \left(\frac{1}{R_s}\right) \tag{8}$$

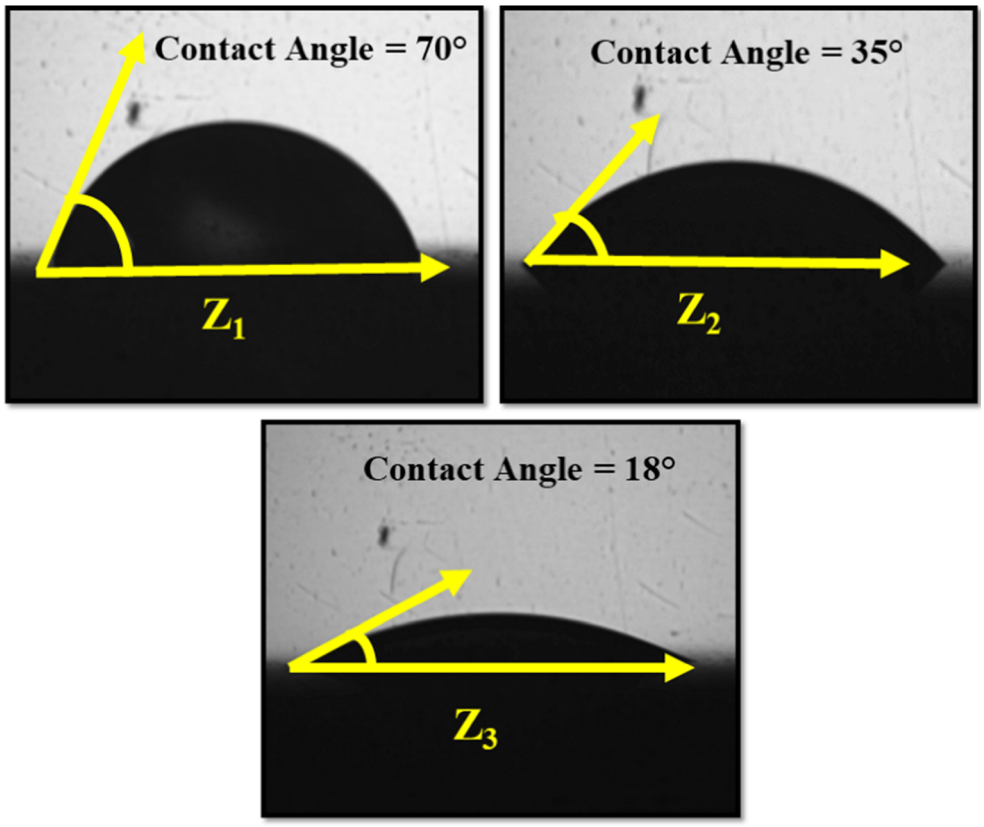

Fig. 5 The contact angle of Z_1, Z_2 and Z_3 thin films

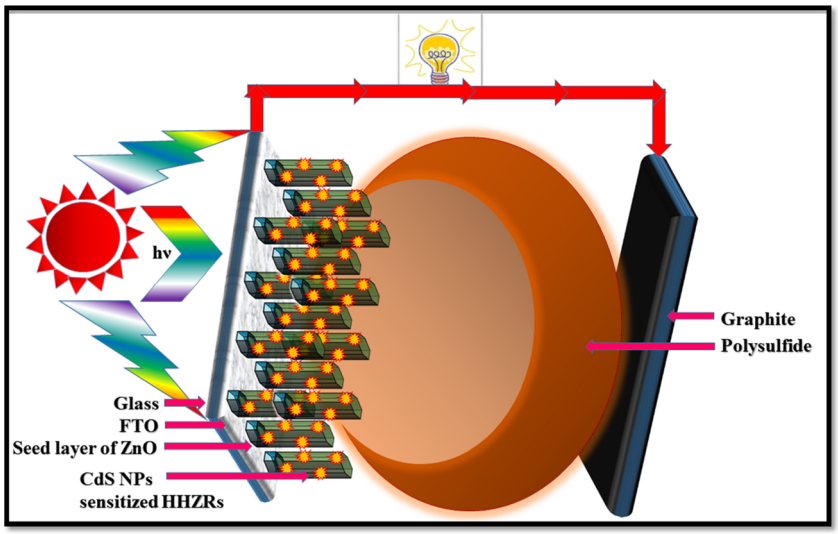

Fig. 6 Schematic diagram of photoelectrochemical performance of Glass/FTO/CdS NPs sensitized HHZRs/0.5 M polysulfide/graphite solar cell assembly under 20 mW cm^{-2} illumination

$$\left(\frac{dI}{dV}\right)_{V=0} = \left(\frac{1}{R_{sh}}\right) \tag{9}$$

Different solar cell parameters that are obtained from the power output are tabulated in Table 1. The minor value of R_{Sh} in the case of all samples is responsible for the deviation from the ideal *I–V* characteristics and therefore the values are observed at low fill factor. R_S varies from 378 to 448 Ω, while R_{Sh} changes from 1.054 to 1.105 kΩ. The Z_3 sample with the maximum photoconversion efficiency of 0.40% is obtained. Such significant increment in current is due to the decoration of CdS over 1-D HHZRs which provides a large surface area to increase the interfacial reaction sites for additional light absorption in the visible region to improve the *I–V* performance. Also, the 1-D structure of HHZRs provides an easy charge transportation with a decrease in the recombination of charge carriers [24]. The uniform, compact morphology decreases the constraints of the grain boundary to make an accessible easier path for the flow of current and by raising the electron diffusion length. Enhancement of photocurrent for the Z_3 sample is also because of its hydrophilic nature which allows easy insertion of electrolyte in the photoelectrode and is beneficial for superior electron transport.

We have faith in that the simplicity and flexibility of the synthesis methods will expose additional chances for fabricating various architectures, which allows structural control on the electron extraction, interface, optical scattering, conduction-band position as well as recombination dynamics for solar cells.

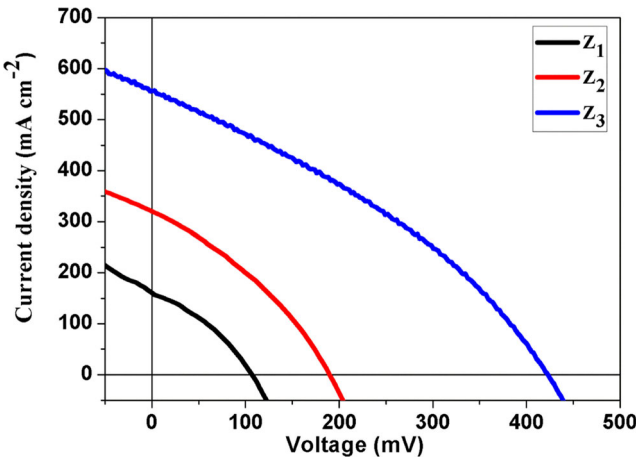

Fig. 7 I–V measurement of Z_1, Z_2 and Z_3 thin films

Electrochemical impedance spectroscopy analysis

Nyquist plot

In the present study, electrochemical impedance spectroscopy (EIS) was used to understand the effect of resistance in the PEC cells and inspect the changes that happen during the illumination. To obtain additional information of charge transfer taking place across semiconductor-redox electrolyte interface, the EIS studies were carried out. EIS study of the ZnO sample (Z_1 and Z_3) electrode was conducted under the illumination using the same system used for PEC measurement as given in Equations. (3) and (5) respectively. Impedance data were recorded using AUTOLAB PGSTAT100 FRA 32 potentiostat at room temperature in the frequency range of 100 KHz–0.1 Hz, by applying an AC potential to an

Table 1 Solar cell output parameters of all the Z_1, Z_2 and Z_3 samples

Sr. No.	Sample code	I_{SC} (μA cm^{-2})	V_{OC} (mV)	I_m (μA cm^{-1})	V_m (mV)	*FF*	R_S (Ω)	R_{Sh} (Ω)	η (%)
1.	Z_1	167	105	82	71	0.33	424	1054	0.03
2.	Z_2	318	190	115	180	0.34	448	1105	0.10
3.	**Z_3**	**558**	**423**	**306**	**259**	**0.34**	**378**	**1058**	**0.40**

electrochemical system and consequently recording the shift in phase and amplitude (0.01 V RMS) of the resultant current response.

The impedance plot includes the response of the counter electrode as well as the photoanode, as the EIS was measured in the two-electrode system. Usually, impedance data were characterized by the complex-plane impedance called Nyquist plot. The Nyquist plot for the Z_1 and Z_3 samples is shown in Fig. 8 (a). *Inset* of Fig. 8 (a) shows the equivalent circuit and summarizes the electrochemical parameters acquired by best fitting the impedance data and are summarized in Table 2. The equivalent circuit elements involve R_S, R_1, C_1, R_2 and C_2. The high-frequency (analogous to low Z′) intercept on the *z*-axis symbolized the series resistance (R_S). R_S are the ohmic series resistance of the electrode system which adds to the electrical contact of the electrode-electrolyte and resistivity of an electrolyte solution. R_1 signifies the charge transfer resistance, and the double layer capacitance is specified by C_1 at the electrode-electrolyte boundary. R_2 is recombination charge transfer resistance and C_2 is the chemical capacitance at the electrode-electrolyte boundary.

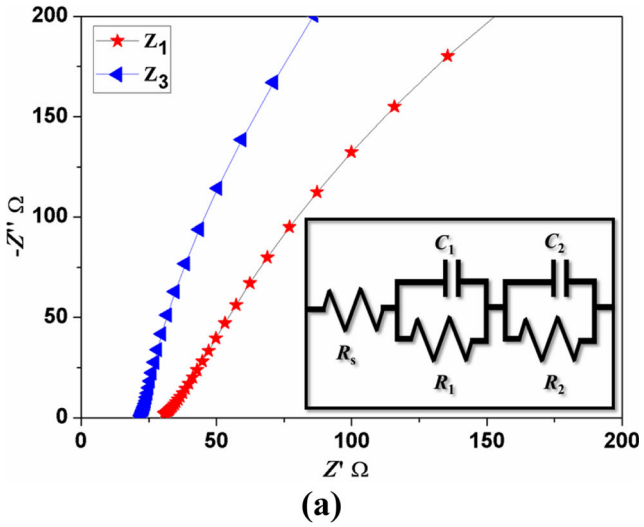

Fig. 8 **(a)** Nyquist plot of Z_1 and Z_3 samples. *Inset* shows the equivalent circuit of the PEC cell. **(b)** Bode plot of Z_1 and Z_3 samples

Table 2 EIS parameters calculated for the ZnO samples (Z_1 and Z_3)

Sample code	R_S (Ω cm^{-2})	R_1 (Ω cm^{-2})	C_1 (μF cm^{-2})	R_2 (Ω cm^{-2})	C_2 (μF cm^{-2})	τ (mS)
Z_1	28	252	21	5546	74	1.17
Z_3	**21**	**961**	**257**	**980**	**900**	**7.97**

R_S value for the Z_1 and Z_3 electrodes are in the order of ohms and reduced after semiconductor sensitization. From Table 2, it is seen that after CdS NPs sensitization, R_S decreases from 28 to 21 Ω cm^{-2}. The small value of C_1 for the Z_3 sample is an indication of a uniform distribution of current through bulk electrode while the increase in C_2 shows the rise in the gathering of charges in the interfacial region. The EIS results are in good accordance with the PEC results.

Bode plot

Figure 8 (b) shows Bode plot which gives the information of electron lifetime inside the PEC cell assembly under illumination. The electron life times for ZnO samples (Z_1 and Z_3) are given in Table 2. In the Bode plot, we obtained log*f* values corresponding to a maximum frequency of the ZnO samples (Z_1 and Z_3). Then taking exponential of (2.303 × log *f*), we can get the *f* value, which can be used to calculate the electron lifetime using formula as,

$$\tau = \frac{1}{2\pi f} \tag{10}$$

The value of electron life time is found to be increased for the Z_3 sample compared with the Z_1 sample. The increase in efficiency for the Z_3 sample is in good agreement with the higher lifetime value of photoelectrons.

Capacitance-voltage (C-V) characteristics

The measurement of capacitance as a function of applied dc voltage is analyzed with Mott-Schottky (M-S) plot. It provides different physical parameters about photoelectrodes [25]. Figure 9 shows the M-S plot of the Z_1 sample. The V_{fb} of a semiconductor is a key aspect in explaining the charge transfer procedure across the semiconductor-electrolyte junction of the PEC cell. The V_{fb} for sample Z_1 can be attained by using M-S relation [21],

$$\frac{1}{C_{SC}^2} = \frac{2}{q\varepsilon_o\varepsilon_S N_D}\left[V - V_{fb} - \frac{K_B T}{q}\right] \tag{11}$$

where ε_o is the permittivity of free space, ε_s is the permittivity of the semiconductor electrode (for ZnO $\varepsilon_s = 8.5$), $q =$

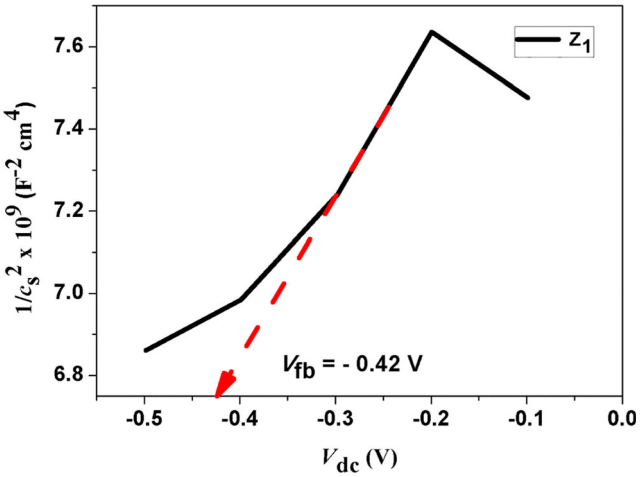

Fig. 9 Mott-Schottky plot of the Z_1 thin film for the capacitance-voltage analysis

1.6021×10^{-19} C is the charge on the carriers, N_D is the donor concentration, T is the temperature of operation ($T \approx 27$ °C), K_B is the Boltzmann's constant, and C_{SC} is the space charge capacitance. The intercept of linear plot at $C_{sc}^2 = 0$ shows that the flat band potential (V_{fb}) is found to be − 0.42 V SCE^{-1}. The donor concentration (N_D) was evaluated from the slope of the M-S plot using the equation,

$$N_D = \left[\frac{2}{\varepsilon_o \varepsilon_s q\ (\text{Slope})}\right] \tag{12}$$

Hence, from the M-S analysis, we conclude that the ZnO is an *n*-type semiconductor. The several significant parameters of the semiconductor determined from M-S plots are given in Table 3.

Theoretical modeling: energy band diagram of Z_1 PEC cell

To evaluate the relative positions of valence band edge, it is necessary to know the positions of the fermi level of redox electrolyte ($E_{f\text{-redox}}$) and semiconductor electrode (E_f) [26]. We can simply show positions of conduction band edge, fermi level and band bending. The density of states in the conduction band (N_c) is calculated using the equation,

$$N_c = \left(\frac{2}{h^3}\right)\left(2\pi m_e^* kT\right) \tag{13}$$

where m_e^* is the effective mass of material. Baer [27] reported the value of m_e^* for ZnO is $0.24 \times m_o$ (where m_o is rest mass of electron). The value of N_c for the Z_1 thin film in the conduction band is 8.11×10^{18} cm^{-3}. As discussed above in Equation (12), the value of N_D is 5.09×10^{13} cm^{-3} for the Z_1 sample. The energy separation between semiconductor conduction band edge and fermi energy that is $(E_c - E_f)$ is calculated using the relation,

$$E_c - E_f = -KT\ln\left(\frac{N_D}{N_C}\right) \tag{14}$$

where E_c is conduction band energy level, E_f is fermi level and E_V is valence band energy level. The value of $(E_c - E_f)$ is found to be 0.28 eV SCE^{-1}. Here, E_C can be calculated as,

$$E_C = V_{fb} - (E_c - E_f) \ldots\ldots (\text{for n-type semiconductor}) \tag{15}$$

This shows that the E_f of the Z_1 thin film is situated at 0.28 eV/SCE below the conduction band edge. From optical absorption studies, the band gap value of the Z_1 sample is obtained to be 3.28 eV. The redox level of the electrolyte ($E_{f\text{-redox}}$) has been determined experimentally and for 0.5 M Na_2SO_4 which is observed to be − 0.18 V/SCE. The band bending (V_{bb}) was evaluated from the relation,

$$V_{bb} = \frac{V_{f\text{-redox}}}{q} - V_{fb} \tag{16}$$

The V_{bb} at Z_1/Na_2SO_4 electrolyte interface is attained by the difference of the $E_{f\text{-redox}}$ and V_{fb} of the semiconductor

Table 3 Summary of results obtained from Mott-Schottky plot of the Z_1 thin film

Sr. No.	Physical parameter	Obtained value for Z_1 thin film
1.	Flat band potential (V_{fb} (*V*/SCE))	− 0.42
2.	Redox electrolyte	0.5 M Na_2SO_4
3.	Redox fermi potential ($E_{f\text{-redox}}$ (*V*/SCE))	− 0.18
4.	Donor density (N_D (cm^{-3}))	5.09×10^{13}
5.	Density of states inside conduction band (N_C (cm^{-3}))	8.11×10^{18}
6.	E_c–E_f (eV/SCE)	0.28
7.	Conduction band boundary (E_c (eV/SCE))	− 0.70
8.	Band bending (V_{bb} (eV/SCE))	0.24
9.	Band gap energy (E_g (eV))	3.28
10.	Valence band boundary (E_v (eV/SCE))	2.58
11.	Barrier height (V_B)	0.52
12.	Type of carrier	*n*-type

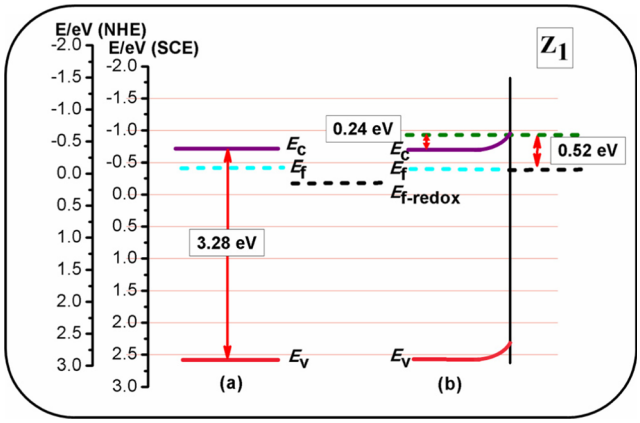

Fig. 10 Theoretical modeling of energy band diagram of Z_1 PEC cell. **(a)** Energy band diagram for Z_1 electrode before contacting the electrolyte. **(b)** Band-bending plot drawn with the values of V_{bb} and V_B

in the equivalent electrolyte, which is estimated to be 0.24 eV/SCE for the Z_1 electrode. The relation for barrier height (V_B) is,

$$V_B = V_{bb} + (E_c - E_f) \tag{17}$$

So, V_B becomes 0.52 eV/SCE for Z_1. Figure 10 (a) show the energy band diagram for the Z_1 electrode before contacting the electrolyte. The band-bending plot drawn with the values of V_{bb} and V_B, which is shown in Fig. 10 (b). The different physical parameters obtained for theoretical modeling of Z_1 sample are mentioned in Table 3.

Conclusions

We have successfully synthesized thin films of pristine 1-D HHZRs, Eosin-Y dye, and CdS semiconductor NPs sensitized 1-D HHZRs. XRD analysis confirmed the formation of ZnO and CdS. The optical band gap values varied from 3.28 to 3.03 eV for the Z_1, Z_2 and Z_3 samples. It is seen that the contact angle of CdS NPs sensitized 1-D HHZRs is hydrophilic in nature, which is beneficial for the charge transportation to FTO substrate. Sensitization shifts the optical absorbance in visible region which is responsible for the improvement in the PEC performance. The overall study suggests that the formation of 1-D hollow hexagonal shaped ZnO rods is advantageous for improving the power conversion efficiency. In conclusion, the use of easy and low-cost preparative technique may pave the way for a promising applicant for third generation photovoltaic devices.

Acknowledgements The authors PSP and SDK are very much thankful to the University Grants Commission (UGC), New Delhi, for the financial support through its project No. 43-517/2014(SR).

References

1. Dresselhaus MS, Thomas IL (2001) Alternative energy technologies. Nature 414(6861):332–337
2. Green MA (2007) Thin-film solar cells: review of materials, technologies and commercial status. J Mater Sci Mater Electron 18: 15–19
3. Tarwal NL, Shinde VV, Kamble AS, Jadhav PR, Patil DS, Patil VB, Patil PS (2011) Photoluminescence and photoelectrochemical properties of nanocrystalline ZnO thin films synthesized by spray pyrolysis technique. Appl Surf Sci 257(24):10789–10794
4. Tarwal NL, Patil PS (2010) Superhydrophobic and transparent ZnO thin films synthesized by spray pyrolysis technique. Appl Surf Sci 256(24):7451–7456
5. Kong XY, Wang ZL (2003) Spontaneous polarization-induced nanohelixes, nanosprings, and nanorings of piezoelectric nanobelts. Nano Lett 3(12):1625–1631
6. Martinson ABF, Elam JW, Hupp JT, Pellin MJ (2007) ZnO nanotube based dye-sensitized solar cells. Nano Lett 7(8):2183–2187
7. Kamble A, Sinha B, Chung K, More A, Vanalakar S, Hong C, Kim J, Patil P (2015) Facile linker free growth of CdS nanoshell on 1-D ZnO: solar cell application. Electron Mater Lett 11(2):171–179
8. Rani S, Suri P, Shishodia PK, Mehra RM (2008) Synthesis of nanocrystalline ZnO powder via sol-gel route for dye-sensitized solar cells. Sol Energy Mater Sol Cells 92(12):1639–1645
9. Basyooni MA, Shaban M, El Sayed AM (2017) Enhanced gas sensing properties of spin-coated Na-doped ZnO nanostructured films. Sci Rep 7:1–12
10. Holmes J, Johnson K, Zhang B, Katz HE, Matthews JS (2012) Metal organic chemical vapor deposition of ZnO from β-ketoiminates. Appl Organomet Chem 26(6):267–272
11. Tarwal NL, Rajgure AV, Inamdar AI, Devan RS, Kim IY, Suryavanshi SS, Ma YR, Kim JH, Patil PS (2013) Growth of multifunctional ZnO thin films by spray pyrolysis technique. Sensors Actuators A Phys 199:67–73
12. Grätzel M (2003) Dye-sensitized solar cells. J Photochem Photobiol C Photochem Rev 4(2):145–153
13. Mali SS, Betty CA, Bhosale PN, Patil PS (2012) Eosin-Y and N3-dye sensitized solar cells (DSSCs) based on novel nanocoral TiO2: a comparative study. Electrochim Acta 59:113–120
14. Kamat PV (2008) Quantum dot solar cells. Semiconductor nanocrystals as light harvesters. J Phys Chem C 112:18737–18753
15. Mali SS, Desai SK, Dalavi DS, Betty CA, Bhosale PN, Patil PS (2011) CdS-sensitized TiO2 nanocorals: hydrothermal synthesis, characterization, application. Photochem Photobiol Sci 10(10): 1652–1658
16. Tak Y, Hong SJ, Lee JS, Yong K (2009) Fabrication of ZnO/CdS core/shell nanowire arrays for efficient solar energy conversion. J Mater Chem 19(33):5945–5951
17. Zhai T, Li L, Ma Y, Liao M, Wang X, Fang X, Yao J, Bando Y, Golberg D (2011) One-dimensional inorganic nanostructures: synthesis, field-emission and photodetection. Chem Soc Rev 40(5): 2986–3004
18. Mali SS, Kim H, Patil PS, Hong CK (2013) Chemically grown vertically aligned 1D ZnO nanorods with CdS coating for efficient quantum dot sensitized solar cells (QDSSC): a controlled synthesis route. Dalt Trans 42(48):16961–16967
19. Kamble AS, Sinha BB, Chung K, Gil MG, Burungale V, Park CJ, Kim JH, Patil PS (2014) Effect of hydroxide anion generating agents on growth and properties of ZnO nanorod arrays. Electrochim Acta 149:386–393
20. Cullity BD, Stock SR (2013) Elements of X-ray diffraction: Pearson new international edition, 3rd edn. Pearson Education Limited

21. Chandra S (1985) Photoelectrochemical solar cells. Gordon and Breach Science Publishers
22. Khot KV, Mali SS, Kharade RR, Mane RM, Patil PS, Hong CK, Kim JH, Heo J, Bhosale PN (2014) Novel-approach for fabrication of CdS thin films for photoelectrochemical solar cell application. J Mater Sci Mater Electron 25:5606–5617
23. Bhat TS, Mali SS, Sheikh AD, Korade SD, Pawar KK, Hong CK, Kim JH, Patil PS (2017) TiO2/PbS/ZnS heterostructure for panchromatic quantum dot sensitized solar cells synthesized by wet chemical route. Opt Mater (Amst) 73:781–792
24. Bhat TS, Devan RS, Mali SS, Kamble AS, Pawar SA, Kim IY, Ma YR, Hong CK, Kim JH, Patil PS (2014) Photoelectrochemically active surfactant free single step hydrothermal mediated titanium dioxide nanorods. J Mater Sci Mater Electron 25:4501–4511
25. Rajpure KY, Bhosale CH (2000) Study of substrate variation effects on the properties of n-Sb2S3 thin film/polyiodide/C photoelectrochemical solar cells. Mater Chem Phys 64(1):14–19
26. Shelke HD, Lokhande AC, Kim JH, Lokhande CD (2017) Photoelectrochemical (PEC) studies on Cu2SnS3 (CTS) thin films deposited by chemical bath deposition method. J Colloid Interface Sci 506:144–153
27. Baer WS (1967) Faraday rotation in ZnO: determination of the electron effective mass. Phys Rev 154(3):785–789